

Received 2 February 2023, accepted 24 February 2023, date of publication 28 February 2023, date of current version 3 March 2023.

Digital Object Identifier 10.1109/ACCESS.2023.3250444

RESEARCH ARTICLE

Lake Experimentation of in-Band Full-Duplex Underwater Acoustic Communications With a Receiving Array

ZHENG GUO¹, AIJUN SONG¹, (Member, IEEE), MOHAMMAD TOWLIAT²,
LEONARD J. CIMINI², (Life Fellow, IEEE), AND XIANG-GEN XIA², (Fellow, IEEE)

¹Department of Electrical and Computer Engineering, The University of Alabama, Tuscaloosa, AL 35487, USA

²Department of Electrical and Computer Engineering, University of Delaware, 139 Newark, DE 19716, USA

Corresponding author: Zheng Guo (zguo18@crimson.ua.edu)

This work was supported by the National Science Foundation under Grant CNS-1704097 and Grant CNS-1704076.

ABSTRACT In-band full-duplex (IBFD) communications is a promising technique to achieve spectral-efficient communication in the underwater environment. To achieve IBFD underwater communications, suppression of self-interference (SI) is a prerequisite. In this paper, SI suppression using physical separation and digital SI cancellation is investigated under different transmitter-receiver geometries. An iterative IBFD receiver combining joint channel estimation, SI cancellation, and multichannel decision feedback equalizer is developed. Due to the potential deterioration of the channel estimation accuracy, a digital SI cancellation control mechanism is used to regulate the suppression process. The feasibility of coherent IBFD underwater acoustic communications was tested in a lake environment. The two SI suppression methods, the SI cancellation control mechanism, and the receiver performance were evaluated using the experimental measurements. A bit error rate (BER) in the order of 10^{-2} was achieved at the range of 80 m for IBFD communications.

INDEX TERMS In-band full-duplex, iterative receiver, self-interference cancellation, underwater acoustic communications.

I. INTRODUCTION

In-band full-duplex (IBFD) communications is a technique that achieves two-way communication between a pair of users using the same frequency band at the same time. By utilizing the same frequency band for the two information streams at each end, IBFD communications has the potential to provide double spectral efficiency [1] relative to half-duplex communications. In addition, simultaneous transmission achieves reduced latency as well. This paper investigates IBFD communications for the underwater environment.

Sufficient self-interference (SI) suppression is the key to realizing IBFD communications. It was long assumed in radio communications that simultaneous receiving and transmitting on the same frequency band was not possible [2]. This assumption captures the most challenging topic of imple-

menting IBFD communications in wireless systems, the SI cancellation. The SI is the inevitable reception from the co-located transmitter during full-duplex transmissions. Due to the significant intensity discrepancy between the SI from the local transceiver and the signal-of-interest (SOI) from the remote transceiver, the interference-corrupted SOI will not support reliable communications if the SI is not sufficiently suppressed. Although the clean digital representation of the SI is known, the imperfect hardware and the complex communication channel can distort the signal in both linear and non-linear ways [3].

The SI cancellation in underwater acoustic communications is facing more challenges than its counterpart in radio-frequency communications, in addition to the aforementioned shared difficulties. The reasons mainly lie in two aspects. First, the reflected multipath SI in the underwater acoustic channel is extensive and highly dynamic [4]. These reflections have significant delay spans [5]. The delay span may

The associate editor coordinating the review of this manuscript and approving it for publication was Tao Wang¹.

extend to tens or even hundreds of symbol intervals. Cancellation of the SI with such a large delay span is a formidable task in underwater acoustics. Second, the bandwidth/carrier-frequency ratio is high in underwater acoustic communications, indicating a broad-band characteristic. As a result, the narrow-band SI cancellation techniques, such as these proposed in radio IBFD communications [6], may not be applicable to underwater acoustic IBFD communications.

A number of efforts have been reported to investigate underwater acoustic IBFD communications. Most of these investigations were focused on the physical layer in three aspects: understanding the SI, developing the SI cancellation algorithms, and designing IBFD receivers. It was found that the performance of the SI suppression deteriorated at high carrier frequencies [7]. The time-varying channel fluctuations [8], [9] were found to cause this deterioration. The acoustic multipath reflections of the SI were characterized [10]. The SI under different experimental geometries, signal formats, and receiver configurations was analyzed [5]. In addition, the SI with the compact-size modem was simulated [11].

Active SI cancellation [12] commonly generates a cancellation signal to null the received SI. Passive SI cancellation [13] minimizes the reception from the local transmitter by methods such as isolation and absorption. Both techniques have been developed for underwater environments. Several active SI cancellation algorithms were developed for underwater acoustic IBFD systems. To separate SI from the remote transmission, a time-reversal method [14] was proposed. Both digital and analog methods were examined for their effectiveness in suppressing SI [4] through simulations. A sparse-constrained maximum likelihood channel estimation algorithm was designed for digital SI cancellation [15]. The stable and time-varying SI components were suppressed separately in a two-stage SI cancellation algorithm [16]. The nonlinear SI was also investigated. The nonlinear SI was resolved by using the output from the power amplifier as the reference signal [17]. In addition, the nonlinear distortion caused by the power amplifier and pre-amplifier was suppressed by an over-parameterization-based recursive least-squares (RLS) algorithm [21] and a Legendre-polynomial-based adaptive filter [18], respectively. A recent effort [19] claimed an 80 dB suppression by analog cancellation with a secondary transmitter for noncoherent transmissions. The passive SI cancellation using beamforming has also been investigated. The vector sensor and phased array transducer were combined to suppress SI in the spatial domain [20]. However, the passive SI cancellation using physical separation has not been examined thoroughly in underwater acoustic IBFD systems.

Multiple underwater acoustic IBFD receivers have been reported. An asynchronous IBFD underwater acoustic communications system was developed [21]. This receiver was tested in a confined pool environment installed with wedge absorbers of high absorption coefficients. The RLS-based receivers [22], [23] were proposed and evaluated in computer

simulations. Another effort [24] reported full-duplex communications at the range of 130 m with a water depth of 40 m, with a noncoherent frequency-shift keying modulation. The reported data rate was 200 bps. The question whether underwater acoustic IBFD communications is feasible or not in open water environments still remains unanswered.

In this paper, the following four issues are investigated: 1) Near-field SI characterization, 2) SI cancellation, 3) IBFD receiver development, and 4) lake experimental evaluation of underwater IBFD communications. Near-field SI characteristics are investigated based on the experimental data. In full-duplex radios [3], the SI is 110 dB above the noise level; however, this intensity difference decreases to around 70 dB in underwater acoustics for 4-meter-separated transmitter and receiver [7]. The difference between RF and underwater IBFD systems leads to different SI cancellation requirements in achieving IBFD communications. SI intensity requirement for IBFD applications in underwater acoustic communications has not been well surveyed. The SI propagates to the local receiver within only a few meters. Limited knowledge about near-field SI propagation is available. In this regard, it is worthwhile to explore the SI characteristics and its cancellation. In this paper, further investigation on SI intensity is reported for different transmitter-receiver (TX-RX) separations. The SI reduction at different physical separation distances is analyzed.

A multichannel iterative IBFD receiver is presented. The receiver combines the joint channel estimation, SI cancellation, and decision-feedback equalization. The SI and SOI impulse responses are jointly estimated to improve the estimation accuracy. Joint channel estimation, SI cancellation, and equalization are iteratively performed. With iterative processing, the detected SOI symbols are applied to refine the quality of the SI and SOI channel estimation. The enhanced channel estimation, in turn, improves the SI cancellation performance and the SOI symbol detection. Multichannel combining [27], [28] is adopted to exploit the spatial diversity of the SOI receptions and enhance the SI cancellation performance. Field experiments are conducted for feasibility verification of underwater acoustic IBFD communications.

The contributions of our work are explained as follows. Performance of digital SI cancellation is evaluated. The deteriorated performance of digital SI cancellation is observed when the TX-RX separation increases. Since increased physical isolation benefits the SI attenuation but deteriorates the digital SI cancellation performance, the choice on the physical separation is discussed. Even though there has already been a study analyzing the impact of signal intensity on interference cancellation in radio full-duplex communications [25], observations with only digital cancellation in underwater acoustics have not been addressed in the existing literature.

Unlike most previous works based on SI-only receptions, the digital SI cancellation performance is investigated in the presence of SOI. With both theoretical derivation and experimental evaluation, the phenomenon that the presence

of SOI deteriorates the digital SI cancellation performance is explained. Instead of treating the SOI as a background noise [26], joint SI and SOI channel estimation is adopted in this work.

A SI cancellation control method is developed in the receiver. It is intuitive that the digital SI cancellation may degrade the receiver performance when the SI channel estimation error is large. Therefore, the SI cancellation control is introduced to ensure a proper application of digital SI cancellation.

The feasibility of IBFD underwater acoustic communications is verified via a lake experiment. The receiver performance is tested with different SI source levels at two communication ranges. To the best of the authors' knowledge, this is the first effort confirming the feasibility of coherent IBFD underwater acoustic communications in field tests.

The nonlinear SI component, in-phase and quadrature mismatch/imbalance, and phase noise are not considered in this paper. When the precision of the digital hydrophones is high, the influence of the analog-to-digital converters (ADC) on digital SI cancellation can be neglected. The adopted hydrophones sample the received waveform with a 24-bit Sigma-Delta ADC, which allows a dynamic range of 132 dB. The maximum achievable SI suppression and the maximum interference-to-noise ratio (INR) are far smaller than this dynamic range. The INR represents the intensity ratio between the SI and noise. The dynamic range thus does not limit the SI cancellation performance.

The rest of the paper is organized as follows. Section II presents the signal model for the IBFD system. Section III presents the iterative IBFD receiver. Analytic expressions of the jointly estimated SI and SOI channel impulse responses are given. The SI cancellation control is introduced. Section IV presents the SI suppression performance evaluation by physical separation and digital SI cancellation. The impact of SOI on SI suppression deterioration is analyzed. The jointly estimated SI and SOI impulse responses from the IBFD receptions are presented. The demodulation results at two communication ranges are shown. Section V concludes the paper.

Throughout this paper, uppercase boldface letters denote matrices. Lower boldface letters denote vectors. The notations $(\cdot)^\dagger$, $(\cdot)^T$, and $(\cdot)^H$ represent pseudo-inverse, transpose, and Hermitian transpose, respectively. The expectation operation is denoted by $\mathbb{E}[\cdot]$. The absolute value is $|\cdot|$. The l_2 norm is $\|\cdot\|_2$. The convolution operation is “*”. The zero vector is $\mathbf{0}$. In addition to INR, several terms are used throughout this paper. The signal-to-noise ratio (SNR) is defined as the intensity ratio between SOI and noise. The signal-to-interference ratio (SIR) denotes the intensity ratio between SOI and SI.

II. SYSTEM MODEL

Acoustic IBFD communications allows transceivers to exchange information using the same frequency band simultaneously. The IBFD transceiver also receives the transmis-

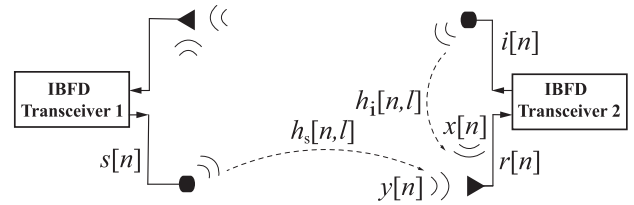


FIGURE 1. Signal model of the IBFD system.

sions from another transceiver while transmitting. Therefore, the self transmission is treated as interference to the remote transmission that needs to be detected. The considered acoustic transmission system consists of two transceivers, each with a transmitter and a receiver. As illustrated in Fig. 1, the received full-duplex signal for Transceiver 2 contains transmissions from both Transceivers 1 and 2. The received baseband signal is given by

$$\begin{aligned} r[n] &= x[n] + y[n] + w[n] \\ &= i[n] * h_i[n, l] + s[n] * h_s[n, l] + w[n], \end{aligned} \quad (1)$$

where $x[n]$ denotes the SI, that is the local transmission, $y[n]$ represents the SOI, or is the remote transmission, $w[n]$ represents the noise, $i[n]$ represents the SI symbols, $s[n]$ represents the SOI symbols, $h_i[n, l]$ and $h_s[n, l]$ represent the SI and SOI channel impulse responses at the arrival index of l for the discrete-time index of n , respectively. It is noted that synchronization of IBFD signals is not addressed in the paper.

The IBFD reception is processed in a blockwise manner. Both the SI and SOI impulse responses are assumed to be static within one processing block. In one processing block, the received signal in (1) can be rewritten in a vector-matrix form as

$$\mathbf{r} = \mathbf{x} + \mathbf{y} + \mathbf{w} = \mathbf{A}_i \mathbf{h}_i + \mathbf{A}_s \mathbf{h}_s + \mathbf{w}, \quad (2)$$

where $\mathbf{r} \in \mathbb{C}^{M \times 1}$ and $\mathbf{r} = [r[n+M-1], r[n+M-2], \dots, r[n]]^T$, $\mathbf{A}_i \in \mathbb{C}^{M \times L_i}$ is the convolution matrix consisting of $i[n]$, $\mathbf{A}_s \in \mathbb{C}^{M \times L_s}$ is the convolution matrix consisting of $s[n]$, $\mathbf{h}_i \in \mathbb{C}^{L_i \times 1}$ and $\mathbf{h}_i = [h_i[0], h_i[1], \dots, h_i[L_i-1]]^T$, $\mathbf{h}_s \in \mathbb{C}^{L_s \times 1}$ and $\mathbf{h}_s = [h_s[0], h_s[1], \dots, h_s[L_s-1]]^T$, $\mathbf{w} \in \mathbb{C}^{M \times 1}$ and $\mathbf{w} = [w[n+M-1], w[n+M-2], \dots, w[n]]^T$, M is the block length, L_i and L_s are the lengths of the SI and SOI impulse responses, respectively.

III. THE IBFD RECEIVER

The receiver structure is presented in Fig. 2. The single-channel reception case is extended to a multichannel reception one. The receiver includes the following four components, which are joint channel estimation, SI cancellation, SI cancellation control, and multichannel decision feedback equalizer (DFE). The received signal, the SOI symbols s , and the SI symbols i are applied to estimate the SI and SOI impulse responses. In the pilot, the SOI symbols s are known to the receiver. In the data blocks, s is replaced by the SOI symbol estimates. The estimated SI impulse responses for the K hydrophones are represented by $\hat{\mathbf{h}}_{i,k}$, $k = 1, 2, \dots, K$. The

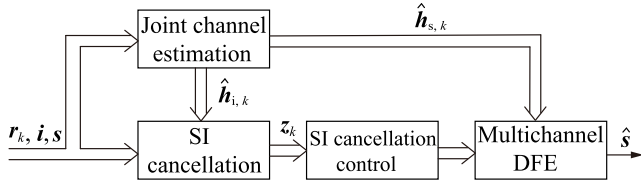


FIGURE 2. IBFD receiver structure.

estimated SOI impulse responses for the K hydrophones are represented by $\hat{\mathbf{h}}_{s,k}$. Next, the received signal, locally transmitted symbols, and the estimated SI impulse responses are used to perform the digital SI cancellation. The signal after SI cancellation is denoted by \mathbf{z}_k . The SI cancellation control is applied to regulate the SI cancellation process. The multichannel DFE is then employed to remove the inter-symbol interference and obtain the SOI symbol estimates, $\hat{\mathbf{s}}$. Note that digital SI cancellation is applied to the reception after physical separation, which is discussed in detail in Sec. IV-B.

A. JOINT CHANNEL ESTIMATION

The least-squares channel estimator is used here to jointly estimate the SI and SOI impulse responses. According to (2), the channel estimator at the k -th hydrophone is denoted as

$$\hat{\mathbf{h}}_k = \mathbf{A}^\dagger \mathbf{r}_k, \quad (3)$$

where $\mathbf{A} = [\mathbf{A}_i, \mathbf{A}_s]$, $\hat{\mathbf{h}}_k = [\hat{\mathbf{h}}_{i,k}, \hat{\mathbf{h}}_{s,k}]^T$, $\mathbf{A}^\dagger = (\mathbf{A}^H \mathbf{A})^{-1} \mathbf{A}^H$. Unless otherwise specified, the hydrophone index k is omitted in the rest of the paper for simplicity.

With derivations from the pseudo-inverse of a column-wise partitioned matrix [29], the jointly estimated SI and SOI impulse responses are denoted by

$$\hat{\mathbf{h}}_i = \mathbf{A}_i^\dagger (\mathbf{I} - \mathbf{A}_s \mathbf{A}_s^\dagger)^\dagger (\mathbf{x} + \mathbf{y} + \mathbf{w}), \quad (4a)$$

$$\hat{\mathbf{h}}_s = \mathbf{A}_s^\dagger (\mathbf{I} - \mathbf{A}_i \mathbf{A}_i^\dagger)^\dagger (\mathbf{x} + \mathbf{y} + \mathbf{w}). \quad (4b)$$

It is seen that both the SI and SOI affect the SI channel estimator and the SOI channel estimator.

B. DIGITAL SI CANCELLATION

Digital SI cancellation involves three steps: estimating the SI impulse response, reconstructing the SI, and subtracting the reconstructed SI from the IBFD signal. The signal after digital SI cancellation, \mathbf{z} , is represented by

$$\mathbf{z} = \mathbf{r} - \hat{\mathbf{x}}, \quad (5)$$

where $\hat{\mathbf{x}} = \mathbf{A}_i \hat{\mathbf{h}}_i$ represents the reconstructed SI. Substituting (2) and (4) into (5) yields

$$\mathbf{z} = \mathbf{P} \mathbf{A}_s \hat{\mathbf{h}}_s + \mathbf{P} \mathbf{A}_i \hat{\mathbf{h}}_i + \mathbf{P} \mathbf{w} \approx \mathbf{A}_s \hat{\mathbf{h}}_s + \mathbf{P} \mathbf{A}_i \hat{\mathbf{h}}_i + \mathbf{P} \mathbf{w}, \quad (6)$$

where $\mathbf{P} = \mathbf{I} - \mathbf{A}_i \mathbf{A}_i^\dagger (\mathbf{I} - \mathbf{A}_s \mathbf{A}_s^\dagger)^\dagger$. The approximation in (6) holds because the SI and SOI symbols are mutually independent, and the observation window for joint channel estimation is long enough. That is, $\mathbf{A}_i \mathbf{A}_i^\dagger (\mathbf{I} - \mathbf{A}_s \mathbf{A}_s^\dagger)^\dagger \mathbf{A}_s \hat{\mathbf{h}}_s \approx \mathbf{0}$.

1) PERFORMANCE METRIC OF THE DIGITAL SI CANCELLATION

The interference cancellation gain [7] (IC gain) is used here to evaluate the performance of the digital SI cancellation. It is defined as the intensity ratio of the SI before and after the SI cancellation,

$$G = \frac{\mathbb{E}[|\mathbf{x}|_2^2]}{\mathbb{E}[|\mathbf{x}_{\text{res}}|_2^2]}, \quad (7)$$

where \mathbf{x}_{res} denotes the residual SI after digital SI cancellation. For IBFD transmissions, it can be approximated by

$$G \approx \frac{\mathbb{E}[|\mathbf{r}|_2^2 - |\mathbf{A}_s \hat{\mathbf{h}}_s|_2^2]}{\mathbb{E}[|\mathbf{z}|_2^2 - |\mathbf{A}_s \hat{\mathbf{h}}_s|_2^2]}. \quad (8)$$

The approximation holds because of the assumption that ambient noise can be neglected in the presence of strong SI and SOI. It is noted that G only measures the intensity change of the SI before and after the digital SI cancellation; the intensity change of the SOI is not revealed.

Another performance metric, SI cancellation factor (SICF), F , is introduced in Ref. 22. The SICF is defined as the ratio of SIRs before and after digital SI cancellation. According to the signal model in (6), the intensity of the SOI after digital SI cancellation is equal to that before digital SI cancellation. The SICF is thus simplified as the intensity ratio of the SI before and after digital SI cancellation. This leads to the equality that $F = G$. This equality yields the conclusion that the SICF and IC gain are identical for the current IBFD receiver. Therefore, only the IC gain is used as the performance metric in the following sections.

2) SI CANCELLATION CONTROL

The SI cancellation control uses the control metric, μ , as the indicator of the digital SI cancellation performance. A threshold of the control metric, $\bar{\mu}$, is further introduced to enhance the SI cancellation control.

The SI cancellation control follows the three steps: 1) the control metric value is calculated after the initial digital SI cancellation, 2) the control metric value is compared with the threshold and the bounds, and 3) SI cancellation decision. If the control metric value falls below the threshold or falls out of the bounds, the digital SI cancellation is suspended. Otherwise, the digital SI cancellation is applied.

The control metric is defined as the intensity ratio of the signals before and after the digital SI cancellation, which is

$$\mu = \frac{\mathbb{E}[|\mathbf{r}|_2^2]}{\mathbb{E}[|\mathbf{z}|_2^2]}. \quad (9)$$

Substituting (10) and (6) to (9) yields

$$\begin{aligned} \mu &= \frac{\mathbb{E}[|\mathbf{A}_s \mathbf{h}_s|_2^2 + \mathbb{E}[|\mathbf{P} \mathbf{A}_i \mathbf{h}_i|_2^2] + \mathbb{E}[|\mathbf{w}|_2^2]}{\mathbb{E}[|\mathbf{A}_s \mathbf{h}_s|_2^2 + \mathbb{E}[|\mathbf{P} \mathbf{A}_i \mathbf{h}_i|_2^2] + \mathbb{E}[|\mathbf{w}|_2^2]} \\ &\approx \frac{\mathbb{E}[|\mathbf{A}_s \mathbf{h}_s|_2^2 + \mathbb{E}[|\mathbf{P} \mathbf{A}_i \mathbf{h}_i|_2^2]}{\mathbb{E}[|\mathbf{A}_s \mathbf{h}_s|_2^2 + \mathbb{E}[|\mathbf{P} \mathbf{A}_i \mathbf{h}_i|_2^2]}. \end{aligned} \quad (10)$$

where the approximation in (10) holds because of the assumption that ambient noise is negligible in the presence of strong SI and SOI. Equation (10) can be further simplified by dividing $\mathbb{E}[\|\mathbf{A}; \mathbf{h}_i\|_2^2]$ as

$$\mu \approx \frac{\alpha + 1}{\alpha + \frac{1}{G}}, \quad (11)$$

where α represents the SIR before digital SI cancellation. According to (7), G should be bounded by $1 < G < \infty$ since the SI intensity after the SI cancellation should always be smaller than that before the SI cancellation. It should be noted that the SI is not suppressed at all when $G \leq 1$. The bounds of the control metric, which is represented by Θ , is thus denoted as

$$\Theta = \left\{ \forall \mu \text{ s.t. } 1 < \mu < 1 + \frac{1}{\alpha} \right\}. \quad (12)$$

Equation (12) states that an upper bound of the control metric after digital SI cancellation is $1 + \frac{1}{\alpha}$. Given the condition that the SOI is weaker than the SI, $\alpha \ll 1$, and the term $\frac{1}{G}$ is ignored from (11), an upper bound of the control metric μ is $\frac{1}{\alpha}$.

Employing the bound only does not guarantee satisfying digital SI cancellation performance, especially when the control metric value falls fairly close to 1. The control threshold, $\bar{\mu}$, is introduced here to enhance the digital SI cancellation performance. Based on the measured SIR and the estimated achievable IC gain, the control threshold $\bar{\mu}$ is calculated from (11). On the other hand, the control metric value should be bounded by (12). With these two conditions, the SI cancellation control is expressed as

$$\zeta = \begin{cases} 1, & \mu \geq \bar{\mu} \text{ and } \mu \in \Theta, \\ 0, & \text{otherwise,} \end{cases} \quad (13)$$

where $\zeta = 1$ indicates that the SI cancellation is applied, $\zeta = 0$ indicates that the SI cancellation is suspended. In field data processing, the estimated achievable IC gain and bound are calculated before the digital SI cancellation process. The estimated achievable IC gain can be calculated by (8) using the pilot where both SI and SOI symbols are known.

C. EQUALIZATION

The channel-estimation-based DFE is applied to remove the inter-symbol interference. The DFE shares the same structure as that presented in Ref. 30, which is used in half-duplex communications. The noise term for the case of IBFD communications is different. Equalization in IBFD communications is based on the signal after the SI cancellation, as given by (6). The composite noise level for the equalizer is the superposition of the residual SI and the noise, which is $\mathbb{E}[\|\mathbf{P}\mathbf{A}; \mathbf{h}_i\|_2^2] + \mathbb{E}[\|\mathbf{w}\|_2^2]$. With the composite noise level expressed above, the DFE is readily extended to the multichannel case where the spatial diversity of the SOI can be exploited.

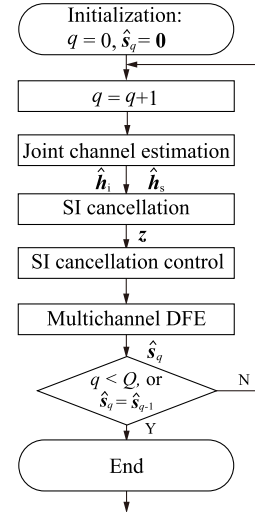


FIGURE 3. Iterative processing for an individual block.

D. ITERATIVE PROCESSING

Fig. 3 presents the flowchart of the iterative IBFD receiver. The iteration count variable, q , and the detected SOI symbols, \hat{s}_q , are initialized to zero. First, the SI and SOI impulse responses are jointly estimated. The estimated impulse responses are used to reconstruct the SI as discussed in Sec. III-B. Note that the digital SI cancellation is only applied to these hydrophones and blocks that are selected by the SI cancellation control. The signal after the digital SI cancellation, together with the estimated SOI impulse responses, are fed to the DFE to obtain the SOI symbol estimates, \hat{s}_q . The iteration is repeated until a specified number of iteration count, Q , is reached or the estimated SOI symbols converge, that is, $\hat{s}_q = \hat{s}_{q-1}$.

In the iteration process, the three sets of estimates, $\hat{\mathbf{h}}_i$, $\hat{\mathbf{h}}_s$, and \hat{s}_q are iteratively updated based on the detected SOI symbols. They, in turn, increase the accuracy of the estimated SI and SOI impulse responses. In addition, these estimates also improve the digital SI cancellation performance. The receiver performance is then improved.

For a K -channel receiver, the complexity equalizing a block of M_3 SOI symbols in each iteration is $\mathcal{O}(K(L_i + L_s)^3) + \mathcal{O}(K(N_{ff} + M_3)L_i^2) + \mathcal{O}(KM_3N_{ff}L_s^2) + [\mathcal{O}(KM_3N_{ff}^3) + \mathcal{O}(M_3N_{fb}N_{ff}^2)]$, in which each term represents the computation cost from joint channel estimation, SI cancellation, SI cancellation control, and DFE equalization, respectively. Note that joint channel estimation is performed only once at each block. The parameters in complexity computation refer to those in Table. 1.

IV. EXPERIMENTAL EVALUATION

Experiments were conducted to evaluate the performance of SI suppression and the iterative receiver. The SI suppression performance is demonstrated first. The impact of physical separation on SI was measured under different experimental configurations. The performance of the digital SI cancellation

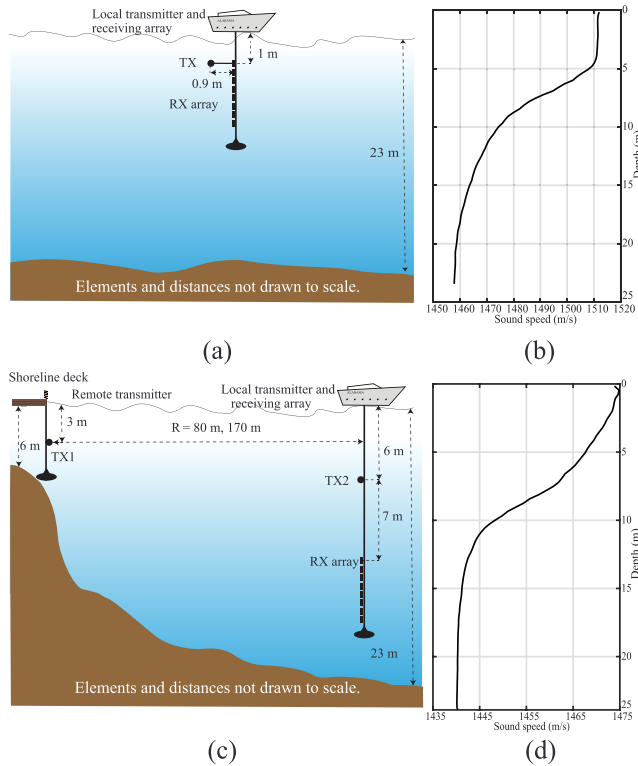


FIGURE 4. Experimental configuration of the two experiments. (a) E1: closely located local transmitter and receiving array and (b) sound speed profile. (c) E2: 7-m-separated local transmitter and receiving array and (d) sound speed profile.

was evaluated with both SI-only and IBFD receptions. The IBFD communication performance is presented next. Effectiveness of the SI cancellation control is demonstrated. The feasibility of IBFD underwater acoustic communications was evaluated at two ranges. Throughout this section, the following metrics were used. The SI intensity level was used as the metric for SI suppression evaluation. The received SI intensity level and the residual SI intensity level are denoted by Γ_r and Γ_{res} , respectively. The bit error rate (BER) and output SNR (OSNR) were used as the metrics for communication performance evaluation. The OSNR represents the intensity ratio between the SOI and noise after equalization. All dB numbers for SOI, SI, and noise intensity levels refer to dB re $1 \mu Pa$.

A. EXPERIMENTAL CONFIGURATION

1) EXPERIMENTAL GEOMETRY

Two experiments were conducted for the IBFD studies. Both experiments were conducted at Lake Tuscaloosa, Tuscaloosa, Alabama. The first experiment, referred to as E1, used a single instrument line and was conducted on Aug 18, 2020. The configuration of experiment E1 is shown in Fig. 4(a). The water depth at the site was 23 m. The instrument line was deployed off a moored boat. It had one acoustic transmitter and a vertical receiving array with eight hydrophones. The transmitter was mounted 1 m below the water surface. The vertical receiving array was horizon-

tally separated from the transmitter by 0.9 m. The eight hydrophones were unequally spaced over 3.2 m. The measured sound speed profile is presented in Fig. 4(b). The instrument line was located at the top layer that had a constant sound speed.

The second experiment, referred to as E2, used two instrument lines and was conducted on Mar 26, 2021. The line with the transmissions to be demodulated is denoted as the remote instrument line. The other one is denoted as the local instrument line. As shown in Fig. 4(c), the remote instrument line, deployed off the shoreline deck, had only a transmitter and was mounted 3 m below the water surface. The water depth was 6 m. The local instrument line was deployed off a moored boat. The water depth at the local instrument line was 23 m. The transmitter was mounted 6 m below the water surface. The separation between the transmitter and the receiving array was 7 m. The eight hydrophones were equally spaced over 2.8 m. The measured sound speed profile is presented in Fig. 4(d). The sound speed profile showed a similar trend across the water column to that in experiment E1, but with a relatively lower speed.

2) ACOUSTIC TRANSMISSIONS

Binary phase-shift keying (BPSK) signals were transmitted in both experiments. The duration of the BPSK signal was 10 s. The center frequency of the transmitted signal was 28 kHz. The symbol rate was 5 kilosymbols/s. Two SI source levels, 174 dB and 154 dB, were tested to measure the SI intensity. In E2, two mutually independent BPSK signals were transmitted simultaneously from the local and remote transmitters at the same frequency band. Two SI source levels for the local transmitter, 174 dB and 164 dB, were tested. The SOI source level remained 174 dB throughout the transmissions. As shown in Fig. 5(a), the designed reception consisted of 5 s SI-only, around 5 s IBFD, and 5 s SOI-only transmissions. An example of the passband reception is presented in Fig. 5(c). The multichannel receptions are listed from the top to the bottom of the receiving array. The presented receptions were with the 174 dB SI source level and the 170 m communication range. Each part of the receptions is marked on the top of the waveforms. The power for the reception from hydrophone H1 is presented in Fig. 5(b). The intensity levels of the SI and SOI visibly varied among the eight hydrophones, but well above the ambient noise intensity level, approximately 83 dB. The intensity levels of the received SOI signals were around 145 dB and 138 dB at 80 m and 170 m, respectively. When the SI source level was 174 dB, the SIRs ranged from -9.6 dB to -0.8 dB for the eight hydrophones at the 80 m communication distance. The SIRs were from -2.5 dB to 2 dB at 160 m. When the SI source level was 164 dB, the SIRs ranged from 3.7 dB to 11.2 dB at 80 m.

B. THE PERFORMANCE OF SI SUPPRESSION

The achieved SI reduction using physical separation and digital SI cancellation is presented. The impact of the SOI on digital SI cancellation performance is discussed.

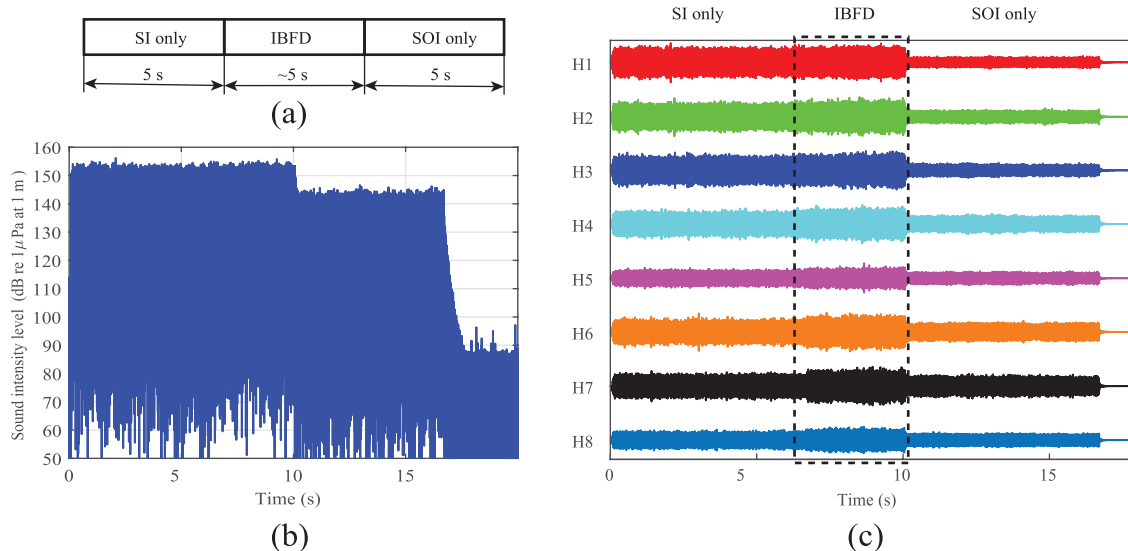


FIGURE 5. Transmission format and acoustic reception. (a) Waveform transmission format, (b) Reception from hydrophone H1, and (c) Passband receptions with y axis indicates the signal amplitude from one packet in E2. The hydrophones (H1 to H8) are listed from the top to the bottom of the receiving array. The receptions were with the 174 dB SI source level and the 170 m communication range. The SOI source level was 174 dB.

1) SI SUPPRESSION WITH THE SI-ONLY RECEPTIONS

The SI suppression using SI-only receptions is investigated first. Fig. 6 presents the measured SI intensity levels from the two experiments. The presented intensity levels were averaged over two packets. The SI reduction with different physical separations is shown. Focus on the received SI intensity levels with the 174 dB SI source level from experiment E1 first. The received SI intensity levels, Γ_r , ranged from 182.4 to 160.9 dB across the hydrophone array. The top two receivers was placed less than 1 m from the transmitter; this resulted in the intensity levels that were higher than the source level. The variation in Γ_r was up to 21.5 dB among the eight receiving elements. Within the 3.2 m TX-RX separation, the intensity level decrease of the SI was significant. Focus on the received SI intensity level with the 174 dB SI source level from experiment E2 next. The received SI intensity levels varied from 152.3 to 149.8 dB from the top to the bottom of the hydrophone array. The variation in Γ_r was up to 2.5 dB across the array elements. The intensity level decrease of the SI with the TX-RX separation between 7 m and 10 m was marginal. The received SI intensity level with the 154 dB SI source level had a similar trend to that with the 174 dB SI source level in both experiments. It was observed that physical separation at 7 m provided up to 32.6 dB SI reduction. No significant variation in Γ_r was observed across the 2.8-m-aperture receiving array in E2. Physical separation beyond 7 m for the investigated results in E2 did not yield extra significant SI reduction.

The performance of digital SI cancellation was evaluated in terms of IC gains. The IC gains were calculated as the difference between Γ_r and Γ_{res} in Fig. 6. Focus on the IC gain with the 174 dB SI source level from experiment E1 first. The achieved IC gains ranged from 33.6 to 18.0 dB

across the eight receiving elements. The IC gain variation was up to 15.6 dB across the array. The IC gains showed a decreasing trend when the receiving elements were placed further away from the transmitter. Focus on the IC gain with the 174 dB SI source level from experiment E2 next. The achieved IC gains ranged from 12.6 to 10.6 dB across the eight hydrophones. The achieved IC gains showed a decreasing trend for increased TX-RX separation. Similar observations were found with the 154 dB SI source level in both experiments.

It is observed that the performance of the digital SI cancellation was impacted by physical separation. The IC gains were higher when the receiving element was placed closer to the transmitter. This phenomenon was seen in both experiments at the two different SI source levels. When the receivers were placed close to the transmitter, a strong direct path existed in the received SI. This strong direct path was relatively stable [10], [16]. It was captured by the channel estimator and canceled by the digital SI cancellation. The stable direct path was weaker when the receiving element was placed farther away from the transmitter. For example, the power of the direct path was 178.7 dB for the top hydrophone in E1 with the 174 dB SI source level; the power of the direct path for the top hydrophone in E2 with the same SI source level was 145.9 dB. This explained why the IC gains in E2 were lower when compared with that in E1. The power of the direct path in the experiment was calculated based on the power delay profile from the estimated channel impulse responses.

It is noted that the IC gains in E1 and E2 showed a significant difference. Take the case with the 174 dB SI source level as an example. The IC gain variation among the eight hydrophones was up to 15.6 dB in E1 in contrast with 2.0 dB

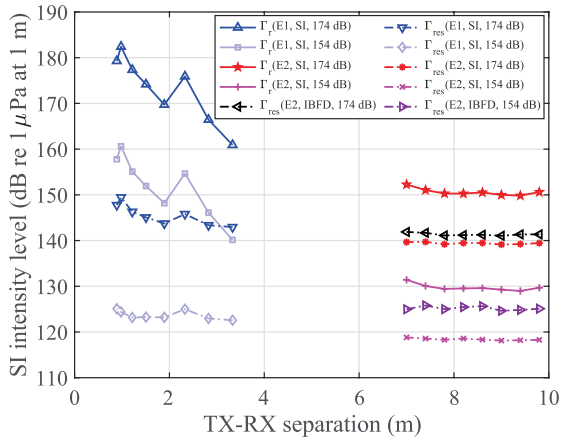


FIGURE 6. Received SI and residual SI intensity levels. The results calculated from the SI-only and IBFD receptions are denoted by SI and IBFD, respectively. The SI source levels are shown inside the brackets of the legend.

in E2. The contrast indicated that the achieved IC gains did not change linearly with the TX-RX separation distance.

The combination of physical separation and digital SI cancellation methods was evaluated. Focus on the residual SI intensity level with the 174 dB SI source level from experiment E1 first. The residual SI intensity levels, Γ_{res} , ranged from 149.5 to 142.9 dB across the eight hydrophones. Up to 6.6 dB difference in Γ_{res} was observed. Focus on the residual SI intensity level with the 174 dB SI source level from experiment E2 next. The residual SI intensity levels ranged from 139.7 to 139.1 dB. The difference was 0.6 dB. The residual SI intensity level with the 154 dB SI source level showed a similar trend in both experiments. The comparison of the residual SI intensity level in both experiments at the 174 dB SI source level revealed that the 7-m physical separation provided up to 10 dB additional SI reduction. Similar observations were also drawn from the case with the 154 dB SI source level.

Increasing the TX-RX separation was beneficial to attenuate the SI. However, this attenuation was limited when TX-RX separation was beyond 7 m. Increasing the TX-RX separation degraded the digital SI cancellation performance. Moreover, increasing the TX-RX separation increases the size of the instrument line. It was thus not worthwhile to increase the TX-RX separation beyond 7 m for the discussed setting.

2) SI SUPPRESSION WITH THE IBFD RECEPTIONS

The SI cancellation performance was evaluated by the IBFD receptions to show the impact of the SOI. Fig.6 presents the digital SI cancellation performance from the IBFD receptions. Compared with the IC gains from the SI-only receptions with the same experimental configuration, the achieved IC gains from the IBFD reception were around 2.0 dB lower at the 174 dB SI source level. This IC gain difference increased to 6.8 dB for the case with the 154 dB SI source

level. The achieved IC gains from the IBFD receptions were low when the SI source level was low. The explanation is that the SOI reduced the estimation accuracy of the SI impulse responses. The accuracy degradation can be explained by the term $A_i^\dagger(I - A_s A_s^\dagger)^\dagger x$ in (4a). With the intensity level of SOI unchanged, the contribution of SI, x , to the SI channel estimator, \hat{h}_i , was reduced with the decreased SI source level. The deviation of the SI channel estimator from the true SI impulse response became more significant when the SI source level was lower. As a result, the reconstructed SI deviated from the true SI and yielded lower IC gains.

C. CHANNEL IMPULSE RESPONSES

The SI and SOI impulse responses during the IBFD transmissions are presented. The impulse responses were jointly estimated according to (4) with true SI and SOI symbols. The acoustic arrivals for the SI impulse responses are marked. All the shown impulse responses were obtained at hydrophone four in E2.

Fig. 7 presents the impulse responses when the SI source level was 164 dB and the communication range was 80 m. The SI arrivals at 60 ms were still strong. This was because the transmitter and receiver were closely located. The surface arrivals after 13 ms showed rapid time variations. Both the SI and SOI impulse responses in Fig. 7 were quite noisy, due to the interference between the SI and SOI.

Fig. 8 presents the impulse responses when the SI source level was 164 dB, and the communication range was 170 m. As expected, the SI impulse responses showed a similar arriving structure to those in Fig. 7(a). The SOI impulse responses were less noisy compared with those in Fig. 7(b). With the decreased SI source level, the impact of the SI on SOI channel estimation became less significant. However, the impact of the SOI on SI channel estimation became more significant. This impact of the SOI was measured by the IC gain as discussed in Sec. IV-B2.

D. IBFD COMMUNICATION PERFORMANCE

The IBFD communication performance was tested at two ranges, 80 m and 170 m. Two SI source levels, which were 174 dB and 164 dB, were tested. The SOI source level was 174 dB throughout the IBFD transmissions. The recordings from the two hydrophones close to the bottom of the receiving array were used to evaluate the two-channel receiver performance. Similarly, the recordings from the four hydrophones close to the bottom of the receiving array were used to evaluate the four-channel receiver performance.

The IBFD receiver operated in the working mode. The pilot, with the length of M_1 , was inserted at the beginning of IBFD transmissions. The data payload following the pilot was processed in a block-wise manner. The ratio of the pilot and data length for the transmission was around 4%. The presented pilot-to-data ratio is for feasibility evaluation purposes; this ratio could be reduced with longer transmitted packets. The detected SOI symbols were used for joint

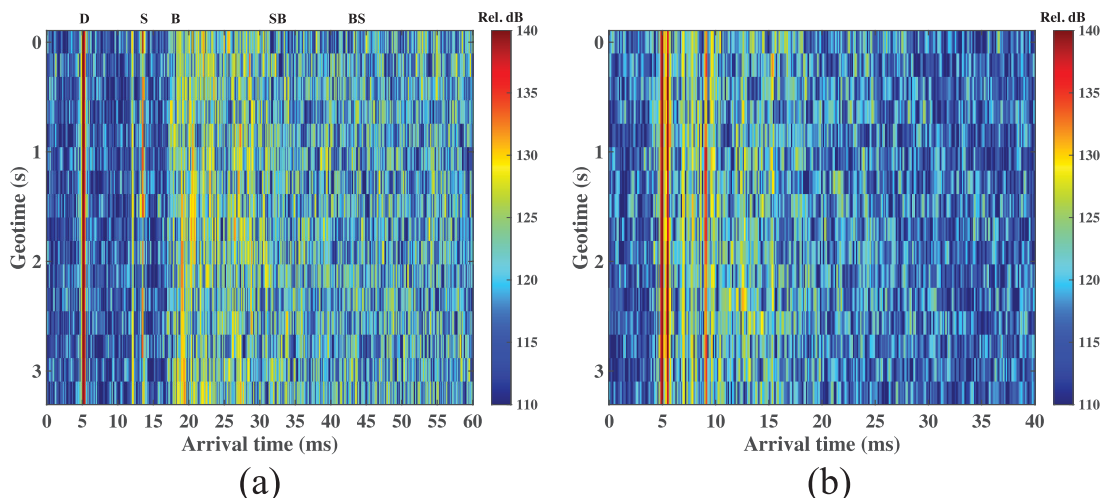


FIGURE 7. SI and SOI impulse responses from one packet with the 174 dB SI source level. The communication range was 80 m. (a) The SI impulse responses and (b) the SOI impulse responses. The travel paths for SI impulse responses are represented by D, S, B, SB, and BS for the direct path, surface reflection, bottom reflection, bottom reflection from the surface, and surface reflection from the bottom, respectively.

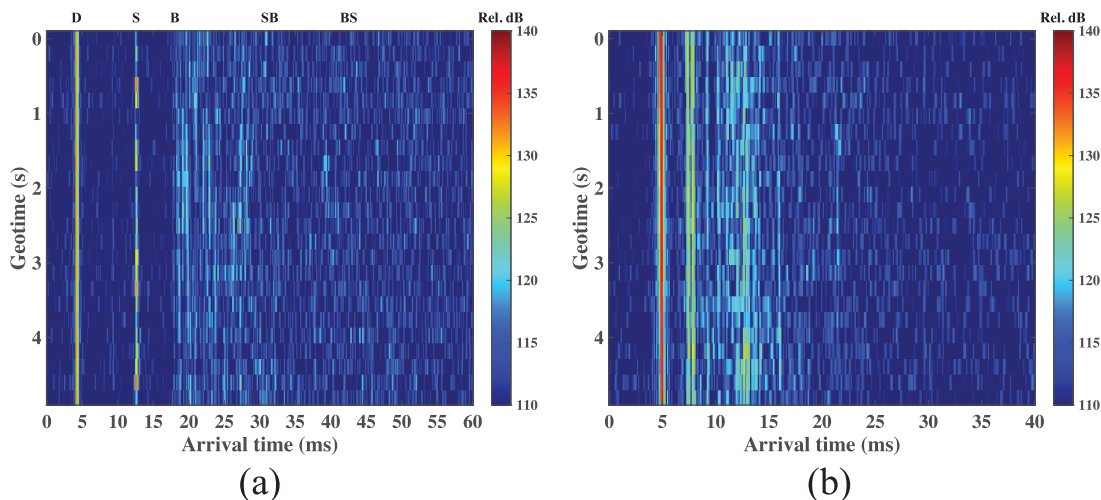


FIGURE 8. SI and SOI impulse responses from one packet with the 164 dB SI source level. The communication range was 170 m. (a) The SI impulse responses and (b) the SOI impulse responses.

channel estimation in each block. The DFE operated in the decision-directed mode. The parameters of the transceiver are listed in Table 1. The threshold least-squares channel estimator was applied. All the arrivals δ dB below the peak arrival were set to zeros. Two different thresholds, 9 and 20 dB, were used for the packets at 80 m and 170 m, respectively. A higher threshold was used for the range of 170 m. This higher threshold allowed more arrivals to be passed to the equalizer. This was necessary when the receptions were weaker. Phase correction [32] was applied to the equalized symbols.

The digital SI cancellation control was employed to ensure the proper suppression of the SI. The SI cancellation was used only when the control metric value was greater than the control threshold, $\bar{\mu}$. Otherwise, the reception without the SI

cancellation was fed to the equalizer. The control threshold was calculated by (11). The IC gain $G = 1.5$ was applied to calculate the control threshold $\bar{\mu}_k$ for the k -th hydrophone.

Fig. 9 presents the receiver performance at two different communication ranges and two different SI source levels. All eight hydrophones were used in the multichannel DFE to detect the SOI symbols. Multiple packets were transmitted in the experiment. Scatter plots from three packets are presented in Fig. 9. Due to the strong SI, the scatter plot at 80 m with the strongest SI source level, 174 dB, had the worst performance, as presented in Fig. 9(a). With a 10 dB SI source level reduction, a better performance was obtained (Fig. 9(b)). The receiver achieved quality demodulation results with the 164 dB SI source level at the range of 170 m; see Fig. 9(c). IBFD communications, with the

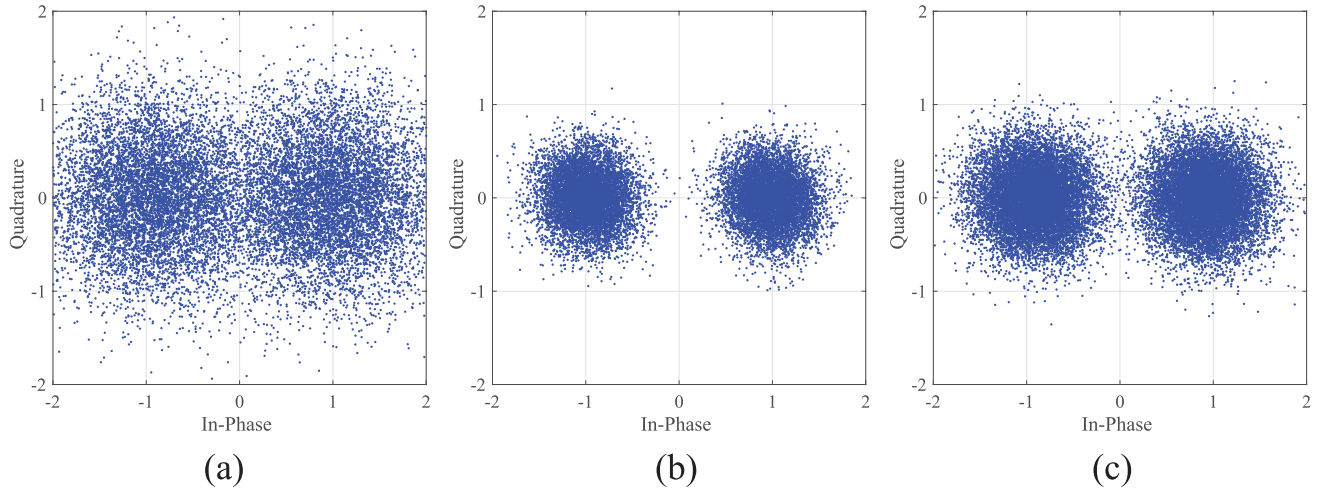


FIGURE 9. Scatter plots of the eight-channel DFE output. Results are shown for (a) the 174 dB SI source level at 80 m communication range, (b) the 164 dB SI source level at 80 m communication range, and (c) the 164 dB SI source level at 170 m communication range.

174 dB SI source level at the range of 170 m, failed when all eight hydrophones were used for demodulation. Due to the attenuation of the SOI at an extended range, the SIRs at 170 m were 3.5 to 10.6 dB lower than that at 80 m with the 174 dB SI source level across the receiving array. This resulted failed communications.

Detailed performance evaluation for the iterative IBFD receiver is presented in Table. 2. Results from two packets are presented for illustrative purposes. The communication performance from other packets was similar and, thus, was omitted. Focus on the case with the 174 dB SI source level at the range of 80 m first. The BERs for the two-channel case were above 0.1. The receiver achieved quality demodulation results with four hydrophones. As expected, the receiver showed the best performance with eight hydrophones. Focus on the case with the 164 dB SI source level at the range of 80 m next, when the SI source level was decreased by 10 dB. The BER decreased as more hydrophones were combined. The BERs were at least one magnitude lower than that when the SI source level was 174 dB.

Focus on the case with the 164 dB SI source level at the range of 170 m last. The receiver failed in the two-channel case. A BER in the order of 10^{-2} was achieved with four hydrophones. The BER was improved by one order of magnitude with eight hydrophones. The receiver achieved IBFD communications at the range of 80 m. For the extended range of 170 m, the receiver established communications with the 164 dB SI source level when more than four hydrophones were used.

It is clear that using multiple receiving elements improved the digital SI cancellation performance. Take the IBFD communication packet with the 174 dB SI source level at the range of 80 m as an example. The digital SI cancellation, which was calculated by (8), in the two-channel case was around 1.3 dB lower than that in the eight-channel case. This was due to the improved channel estimation accuracy resulted from the enhanced symbol detection.

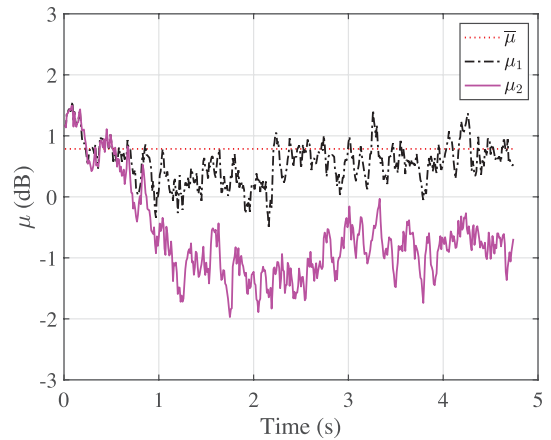


FIGURE 10. The control metric value with and without SI cancellation control for the four-channel receiver from one packet for hydrophone five at the range of 170 m. The control metric values with and without SI cancellation control are denoted by μ_1 and μ_2 , respectively. A total number of 108 blocks were applied with digital SI cancellation for a total number of 474 processing blocks.

The iterative IBFD receiver, when SI cancellation control was not applied, was tested. The effectiveness of the SI cancellation control was shown for two- or four- channel cases. The receiver with the SI cancellation control worked in some cases where its counterpart without the SI cancellation control failed. An example is the four-channel case with the 164 dB SI source level at the range of 170 m. The receiver with SI cancellation control achieved a BER in the order of 10^{-2} while its counterpart without SI cancellation control failed.

The effectiveness of the SI cancellation control was illustrated by the control metric value. Fig. 10 presents the control metric values for packet one at the range of 170 m. Four hydrophones were used for demodulation. Focus on the case when the SI cancellation control was not applied first. The control metric value was above 0 dB at the pilot. As the

TABLE 1. Parameters setting for the transceiver.

Parameters	Description	Value
f_c	Carrier frequency	28 kHz
f_{sr}	Symbol rate	5 kilosymbols/s
f_{os}	Over-sampling factor	2
T_{IBFD}	Duration of the IBFD transmission	~5 s
K	Total number of hydrophones	2, 4, 8
Q	Maximum number of iterations	3
M_1	Discrete length of the pilot	2000
M_2	Length of the channel estimation observation window	2000
M_3	Sliding length in block processing	100
L_i	Length of the SI channel	600
L_s	Length of the SOI channel	400
N_{ff}	Length of the feedforward filter at each hydrophone	600
N_{fb}	Length of the feedback filter at each hydrophone	399
δ	Thresholds for threshold least-squares estimators	9 or 20 dB ^a

^a 9 dB for $R = 80$ m, 20 dB for $R = 170$ m.

TABLE 2. Communication performance.

R (m)	SI source level (dB)	Packet	Metric	K		
				2	4	8
80	174	1	OSNR	-3.1	1.2	3.4
			BER	0.26	6.6e-2	3.1e-2
		2	OSNR	-1.9	0.7	3.5
			BER	0.17	8.4e-2	3.2e-2
80	164	1	OSNR	1.9	5.2	8.7
			BER	4.0e-2	5.7e-3	6.4e-5
		2	OSNR	1.5	6.0	8.9
			BER	4.6e-2	2.6e-3	6.4e-5
170	164	1	OSNR	Fail ^a	2.0	7.5
			BER	Fail	9.7e-2	1.3e-3
		2	OSNR	Fail	3.4	7.9
			BER	Fail	5.1e-2	1.5e-3

^aThe metrics where the BERs are greater than 0.3 are marked as failed [31].

demodulation proceeded, the control metric value quickly fell below 0 dB. This meant that the accuracy of the estimated SI impulse responses deteriorated when the BER was high. The control metric value after 1 s was mostly less than 0 dB in Fig. 10. The SI cancellation did not remove the SI from the IBFD signal. As a result, the receiver failed.

Focus on the case when the SI cancellation control was applied next. The control metric value decreased first as the demodulation proceeded. With the SI cancellation control, the receiver was still able to maintain the above-zero-dB control metric in most blocks. This way, the SI suppression was improved. Similar observations were also found for the other three hydrophones.

E. MAJOR HURDLES IN ACHIEVING IBFD COMMUNICATIONS AT 170 m

SI suppression was the major issue in achieving IBFD communications at 170 m with the 174 dB SI source level. According to the SI analysis in Sec. IV-B2, the achieved digital SI cancellation for IBFD receptions was around 9 dB. Combined with physical separation and digital SI cancellation, the overall achieved SI suppression reached 40.7 dB. As shown in Fig. 11, the residual SI intensity levels, Γ_{res} , were still 0.4 - 6.2 dB above the received SOI intensity

levels. The residual SI intensity levels presented in Fig. 11 were identical to those presented in Fig. 6. The SIRs after physical separation and digital SI cancellation were low. As a result, the SI suppression was not adequate to support IBFD communications at extended ranges. It should also be noted that additional 58 dB SI cancellation is needed to suppress SI to the noise level. This was a difficult task. However, it was shown in Table. 2 that IBFD underwater acoustic communications was feasible if additional 10 dB SI suppression could be achieved at the extended range of 170 m. Therefore, at least 51 dB SI suppression was needed to achieve acoustic IBFD communications at the range of 170 m with the eight-element array. The needed SI suppression was calculated by adding the achieved 40.7 dB with the additional 10 dB SI suppression.

F. FULL-DUPLEX VERSUS HALF-DUPLEX COMMUNICATIONS

IBFD communications was compared with the half-duplex communications. The comparison was based on the BPSK receptions at the range of 80 m in E2. An iterative half-duplex receiver similar to the IBFD receiver in Fig. 2 was used. The half-duplex receiver did not use the SI cancellation and SI cancellation control. The same set of parameters, such as N_{ff}

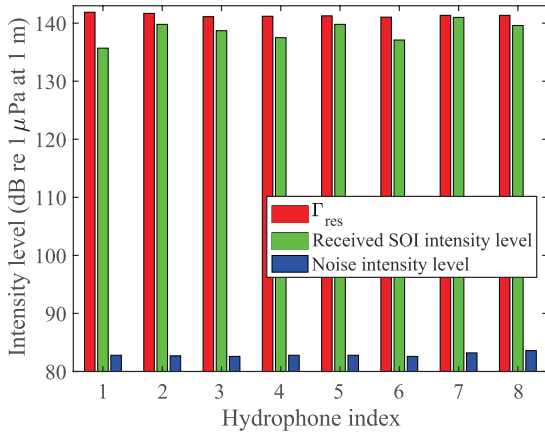


FIGURE 11. Illustration of the signal intensity level measured at the range of 170 m with the 174 dB SI source level. The residual SI intensity level, received SOI intensity level, and noise intensity level are shown.

TABLE 3. Performance of the half-duplex communications at the range of 80 m.

Packet	Metric	K		
		2	4	8
1	OSNR	3.7	7.0	10.0
	BER	1.5e-2	7.1e-4	2.0e-5
	OSNR	3.5	7.3	10.2
2	BER	1.5e-2	3.4e-4	0

and N_{fb} , were used to demodulate the half-duplex receptions. The demodulation shared the same configuration with that in the IBFD demodulation. Results from two packets are shown in Table. 3.

Two metrics, data rate and OSNR, were used to illustrate the advantages and losses in achieving IBFD communications. Both half-duplex and IBFD links were established when more than two hydrophones were used. It was assumed that a remote receiver achieved the same communication performance as the local receiver. The data rate for IBFD communications was then 10 kilosymbols/s, which was double the data rate in half-duplex communications. Take the eight-channel receiver as an example. Around 48 kilosymbols were correctly demodulated in IBFD communications within 5 s, which was 1.9 times those in half-duplex communications. IBFD communications outperformed half-duplex communications in terms of data rates. Turn the focus to the OSNR metric. With the same number of hydrophones for demodulation, it was observed that the OSNR in IBFD communications was around 6 dB lower than that in half-duplex communications. The OSNR was sacrificed for achieving a higher data rate in IBFD communications. If a higher SI suppression gain was attained, this OSNR gap between half-duplex and IBFD communications could be narrowed.

V. DISCUSSION AND CONCLUSIONS

Lake experiments were conducted for the characterization of the SI and feasibility evaluation of underwater IBFD communications. The SI is a key bottleneck in achieving

IBFD underwater acoustic communications. In this paper, both physical separation and digital SI cancellation were investigated. It was found that physical separation at 7 m provided a maximum of 32.6 dB reduction in the SI. Only marginal improvements in the SI reduction were observed when the TX-RX physical separation was extended beyond 7 m.

It is interesting to note that smaller digital SI cancellation gains were achieved at larger separation ranges. Digital SI cancellation achieved up to 33.6 dB SI suppression for the closely located transmitter and receiver at the 174 dB SI source level. In comparison, only 12.6 dB was achieved by digital SI cancellation for the 7-m TX-RX separation. The explanation is the stable direct path was weaker at larger TX-RX ranges. The attenuation of the stable direct path was accountable for the SI cancellation degradation when the TX-RX separation increased.

A combination of a 7-m physical separation and digital SI cancellation obtained up to a 10 dB improvement in SI suppression compared with that with the closely located transmitter and receiver. Increased physical separation benefited the SI attenuation but deteriorated the digital SI cancellation performance and increased the size of the instrumental line. It was not worthwhile to increase the TX-RX separation beyond 7 m for the investigated setting.

Another reported finding is that the existence of the SOI degraded the SI cancellation performance. The IC gain was around 2.0 dB lower than that with the SI-only receptions at the 174 dB SI source level. The degradation extended to 6.8 dB when compared with those with the 154 dB SI source level. This phenomenon can be explained by the decreased channel estimation accuracy when the SOI was present.

An iterative receiver that combined joint channel estimation, SI cancellation, and multichannel DFE was used to recover the transmissions in the IBFD setting. Iterative processing was utilized to enhance communication performance. The receiver used the pilot at the beginning of the packet and was able to detect the SOI symbols in decision-directed mode. At each iteration, joint channel estimation was used to improve the channel estimation accuracy.

Application of the receiving array provided two benefits. First, using multiple channels exploited the spatial diversity of the SOI and, thus, improved symbol detection performance. Second, it improved the digital SI cancellation performance, which resulted from the improved SI channel estimation accuracy and improved symbol detection performance. Both benefits led to enhanced detection performance for the decision-directed receiver.

The SI cancellation control mechanism was essential to ensure the proper SI removal when the channel estimation accuracy deteriorated. The SI cancellation control showed improvements based on the experimental data, in terms of both the OSNR and BER, for a small-sized array. With the SI cancellation control, the developed receiver was still able to work when the receiver without SI cancellation control failed.

The feasibility of coherent IBFD underwater acoustic communications was demonstrated at the range of 80 m in a lake environment. The achieved BER was in the order of 10^{-2} . Compared with the half-duplex communications at the same range, more than 6 dB OSNR was sacrificed to achieve the IBFD communications. This OSNR loss could be reduced if a higher SI suppression gain than what was achieved here could be attained. At the range of 170 m, the attempt to demonstrate acoustic IBFD communications failed. This was partly due to the attenuation of the SOI. The SI suppression gain from the two investigated methods was not adequate. The resulted SIRs were not able to support IBFD communications at the extended ranges.

SI suppression remained a high challenge in acoustic IBFD communications. The time-varying multipath reflections were the fundamental reason for this challenge. With the eight-element receiving array, at least 51 dB SI suppression was needed to achieve acoustic IBFD communications at the range of 170 m. Therefore, both analog and digital cancellation methods should be sought after in future efforts.

ACKNOWLEDGMENT

The authors would like to thank all the participants for their support in conducting the 2020 and 2021 acoustic experiments in Lake Tuscaloosa.

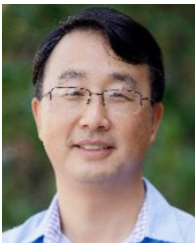
REFERENCES

- [1] D. Kim, H. Lee, and D. Hong, "A survey of in-band full-duplex transmission: From the perspective of PHY and MAC layers," *IEEE Commun. Surveys Tuts.*, vol. 17, no. 4, pp. 2017–2046, 4th Quart., 2015.
- [2] A. Goldsmith, *Wireless Communications*. New York, NY, USA: Cambridge Univ. Press, 2005, Ch. 14, p. 423.
- [3] D. Bharadia, E. McMillin, and S. Katti, "Full duplex radios," *ACM SIGCOMM Comput. Commun. Rev.*, vol. 43, no. 4, pp. 375–386, Sep. 2013.
- [4] L. Li, A. Song, L. J. Cimini, X.-G. Xia, and C.-C. Shen, "Interference cancellation in in-band full-duplex underwater acoustic systems," in *Proc. OCEANS MTS/IEEE Washington*, Oct. 2015, pp. 1–6.
- [5] C. T. Healy, B. A. Jebur, C. C. Tsimenidis, J. Neasham, and J. Chambers, "Experimental measurements and analysis of in-band full-duplex interference for underwater acoustic communication systems," in *Proc. OCEANS Marseille*, Jun. 2019, pp. 1–5.
- [6] T. Snow, C. Fulton, and W. J. Chappell, "Transmit–receive duplexing using digital beamforming system to cancel self-interference," *IEEE Trans. Microw. Theory Techn.*, vol. 59, no. 12, pp. 3494–3503, Dec. 2011.
- [7] Z. Guo, A. Song, M. Towliat, L. J. Cimini, X.-G. Xia, and C.-C. Shen, "Self-interference characterization for in-band full duplex underwater acoustic communications," in *Proc. Int. Conf. Underwater Netw. Syst.*, Oct. 2019, pp. 1–5.
- [8] Z. Guo, A. Song, M. Towliat, L. J. Cimini, and X.-G. Xia, "Impacts of channel fluctuations on least-squares channel estimation in underwater acoustic communications," *J. Acoust. Soc. Amer.*, vol. 149, no. 6, pp. 3929–3942, Jun. 2021.
- [9] Z. Guo, "In-band full-duplex underwater acoustic communications," Ph.D. dissertation, Dept. Elect. Comput. Eng., Univ. Alabama, Tuscaloosa, AL, USA, 2021.
- [10] M. Towliat, Z. Guo, L. J. Cimini, X.-G. Xia, and A. Song, "Self-interference channel characterization in underwater acoustic in-band full-duplex communications using OFDM," in *Proc. Global Oceans, Singapore U.S. Gulf Coast*, Oct. 2020, pp. 1–7.
- [11] G. Qiao, Y. Zhao, S. Liu, and N. Ahmed, "The effect of acoustic-shell coupling on near-end self-interference signal of in-band full-duplex underwater acoustic communication modem," in *Proc. 17th Int. Bhurban Conf. Appl. Sci. Technol. (IBCAST)*, Jan. 2020, pp. 606–610.
- [12] D. Korpi, L. Anttila, V. Syrjala, and M. Valkama, "Widely linear digital self-interference cancellation in direct-conversion full-duplex transceiver," *IEEE J. Sel. Areas Commun.*, vol. 32, no. 9, pp. 1674–1687, Sep. 2014.
- [13] E. Everett, A. Sahai, and A. Sabharwal, "Passive self-interference suppression for full-duplex infrastructure nodes," *IEEE Trans. Wireless Commun.*, vol. 13, no. 2, pp. 680–694, Jan. 2014.
- [14] J. Tian, S. Yan, L. Xu, and J. Xi, "A time-reversal based digital cancellation scheme for in-band full-duplex underwater acoustic systems," in *Proc. OCEANS Shanghai*, Apr. 2016, pp. 1–4.
- [15] G. Qiao, S. Gan, S. Liu, and Q. Song, "Self-interference channel estimation algorithm based on maximum-likelihood estimator in in-band full-duplex underwater acoustic communication system," *IEEE Access*, vol. 6, pp. 62324–62334, 2018.
- [16] L. Shen, B. Henson, Y. Zakharov, and P. Mitchell, "Two-stage self-interference cancellation for full-duplex underwater acoustic systems," in *Proc. OCEANS Marseille*, Jun. 2019, pp. 1–6.
- [17] L. Shen, B. Henson, Y. Zakharov, and P. Mitchell, "Digital self-interference cancellation for full-duplex underwater acoustic systems," *IEEE Trans. Circuits Syst. II, Exp. Briefs*, vol. 67, no. 1, pp. 192–196, Jan. 2020.
- [18] L. Shen, B. Henson, Y. Zakharov, and P. D. Mitchell, "Adaptive nonlinear equalizer for full-duplex underwater acoustic systems," *IEEE Access*, vol. 8, pp. 108169–108178, 2020.
- [19] J. E. Manley, M. Murphree, and G. Folts, "Full-duplex comms, simultaneous transmit, receive for static and mobile nodes," *Sea Tech.*, vol. 59, no. 5, pp. 18–22, May 2018.
- [20] Y.-T. Hsieh, M. Rahmati, and D. Pompili, "FD-UWA: Full-duplex underwater acoustic comms via self-interference cancellation in space," in *Proc. IEEE 17th Int. Conf. Mobile Ad Hoc Sensor Syst. (MASS)*, Dec. 2020, pp. 256–264.
- [21] G. Qiao, S. Gan, S. Liu, L. Ma, and Z. Sun, "Digital self-interference cancellation for asynchronous in-band full-duplex underwater acoustic communication," *Sensors*, vol. 18, no. 6, p. 1700, May 2018.
- [22] L. Shen, Y. Zakharov, B. Henson, N. Morozov, and P. D. Mitchell, "Adaptive filtering for full-duplex UWA systems with time-varying self-interference channel," *IEEE Access*, vol. 8, pp. 187590–187604, 2020.
- [23] M. Towliat, Z. Guo, L. J. Cimini, X.-G. Xia, and A. Song, "An adaptive receiver for underwater acoustic full-duplex communication with joint tracking of the remote and self-interference channels," in *Proc. Global Oceans, Singapore U.S. Gulf Coast*, Oct. 2020, pp. 1–7.
- [24] J. E. Manley, G. Folts, and N. Judell, "DOLPHIN, an emerging technology for undersea acoustics," in *Proc. Global Oceans, Singapore U.S. Gulf Coast*, Oct. 2020, pp. 1–5.
- [25] M. Duarte, C. Dick, and A. Sabharwal, "Experiment-driven characterization of full-duplex wireless systems," *IEEE Trans. Wireless Commun.*, vol. 11, no. 12, pp. 4296–4307, Dec. 2012.
- [26] D. Korpi, L. Anttila, and M. Valkama, "Impact of received signal on self-interference channel estimation and achievable rates in in-band full-duplex transceivers," in *Proc. 48th Asilomar Conf. Signals, Syst. Comput.*, Nov. 2014, pp. 975–982.
- [27] M. Stojanovic, J. Catipovic, and J. G. Proakis, "Adaptive multichannel combining and equalization for underwater acoustic communications," *J. Acoust. Soc. Amer.*, vol. 94, no. 3, pp. 1621–1631, Sep. 1993.
- [28] T. C. Yang, "A study of spatial processing gain in underwater acoustic communications," *IEEE J. Ocean. Eng.*, vol. 32, no. 3, pp. 689–709, Jul. 2007.
- [29] J. K. Baksalary and O. M. Baksalary, "Particular formulae for the Moore–Penrose inverse of a columnwise partitioned matrix," *Linear Algebra Appl.*, vol. 421, no. 1, pp. 16–23, 2007.
- [30] J. C. Preisig, "Performance analysis of adaptive equalization for coherent acoustic communications in the time-varying ocean environment," *J. Acoust. Soc. Amer.*, vol. 118, no. 1, pp. 263–278, Jul. 2005.
- [31] A. Song, A. Abdi, M. Badiey, and P. Hursky, "Experimental demonstration of underwater acoustic communication by vector sensors," *IEEE J. Ocean. Eng.*, vol. 36, no. 3, pp. 454–461, Jul. 2011.
- [32] Y. R. Zheng, "Channel estimation and phase-correction for robust underwater acoustic communications," in *Proc. MILCOM IEEE Mil. Commun. Conf.*, Oct. 2007, pp. 1–6.



ZHENG GUO received the B.S. degree in electro-information engineering of underwater acoustics from Harbin Engineering University, Harbin, China, in 2014, the M.Eng. degree in electronics and communication engineering from the University of Chinese Academy of Sciences, Beijing, China, in 2017, and the Ph.D. degree in electrical engineering from The University of Alabama, Tuscaloosa, USA, in 2021.

He is currently a Senior Wireless System Engineer with NXP Semiconductors, San Jose, CA, USA. His research interests include signal processing, digital communications, and interference mitigation for wireless communication systems.



AIJUN SONG (Member, IEEE) received the Ph.D. degree in electrical engineering from the University of Delaware, Newark, DE, USA, in 2005.

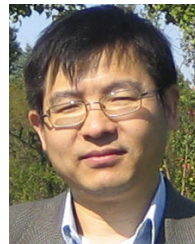
He is currently an Associate Professor with the Department of Electrical and Computer Engineering, The University of Alabama, Tuscaloosa, AL, USA. From 2005 to 2008, he was a Postdoctoral Research Associate with the College of Earth, Ocean, and Environment, University of Delaware. During this period, he was also an Office of Naval Research (ONR) Postdoctoral Fellow, supported by the Special Research Award in the ONR Ocean Acoustics Program. He was a Research Professor with the University of Delaware, from 2008 to 2015. His current research interests include underwater wireless communications and networking, underwater robotics, community-shared open infrastructure for underwater applications, and integrated communications, navigation, and sensing. He was a recipient of the NSF CAREER Award, in 2021. He served as the General Co-Chair for the 2018 March NSF Workshop on Underwater Wireless Communications and Networking and the 2018 November NSF Workshop on Underwater Wireless Infrastructure. He was the General Co-Chair of the 14th International Conference on Underwater Networks and Systems.



MOHAMMAD TOWLIAT received the B.Sc. degree in electrical engineering from Birjand University, Birjand, Iran, in 2009, and the M.S. degree in electrical engineering from the Ferdowsi University of Mashhad, Mashhad, Iran, in 2012. He is currently pursuing the Ph.D. degree with the Department of Electrical and Computer Engineering, University of Delaware, Newark, DE, USA. His general research interests include MIMO multicarrier systems and space-time coding techniques in communications.



LEONARD J. CIMINI (Life Fellow, IEEE) received the Ph.D. degree from the University of Pennsylvania, in 1982. He was with AT&T, first in Bell Laboratories and then AT&T Laboratories, for 20 years. He has been a Professor with the University of Delaware, Newark, DE, USA, since 2002. He was elected as the IEEE Fellow for contributions to the theory and practice of high-speed wireless communications, in 2000. For his pioneering work on OFDM for wireless systems, he was a recipient of the 2007 James R. Evans Avant Grade Award from the IEEE Vehicular Technology Society and the 2010 Innovators Award from the NJ Inventors Hall of Fame. He was also a recipient of several other awards from the IEEE Communications Society, including the 2010 Stephen O. Rice Prize, the 2010 Donald W. McLellan Meritorious Service Award, the 2010 Recognition Award from the Wireless Communications Technical Committee, the 2011 Service and 2021 Technical Achievement Awards from the Communication Theory Technical Committee, the 2016 Joseph LoCicero Award for exemplary service to publications, and the 2021 Mentorship Award from the Women in Communications Engineering Standing Committee. He has held several publications and governance positions within the IEEE Communications Society, including as the Founding Editor-in-Chief of the IEEE JOURNAL ON SELECTED AREAS IN COMMUNICATIONS (JSAC) Wireless Communications Series.



XIANG-GEN XIA (Fellow, IEEE) received the B.S. degree in mathematics from Nanjing Normal University, Nanjing, China, in 1983, the M.S. degree in mathematics from Nankai University, Tianjin, China, in 1986, and the Ph.D. degree in electrical engineering from the University of Southern California, Los Angeles, in 1992.

He was a Senior/Research Staff Member with the Hughes Research Laboratories, Malibu, California, from 1995 to 1996. In September 1996, he joined the Department of Electrical and Computer Engineering, University of Delaware, Newark, Delaware, where he is currently the Charles Black Evans Professor. His current research interests include space-time coding, MIMO and OFDM systems, digital signal processing, and SAR and ISAR imaging. He is the author of the book *Modulated Coding for Intersymbol Interference Channels* (New York, Marcel Dekker, 2000).

Dr. Xia received the National Science Foundation (NSF) Faculty Early Career Development (CAREER) Program Award, in 1997, the Office of Naval Research (ONR) Young Investigator Award, in 1998, and the Outstanding Overseas Young Investigator Award from the National Nature Science Foundation of China, in 2001. He received the 2019 Information Theory Outstanding Overseas Chinese Scientist Award, and the Information Theory Society of Chinese Institute of Electronics. He is the Technical Program Chair of the Signal Processing Symposium, GLOBECOM, Washington, DC, in 2007, and the General Co-Chair of ICASSP 2005 in Philadelphia. He has served as an Associate Editor for numerous international journals, including IEEE TRANSACTIONS ON SIGNAL PROCESSING, IEEE TRANSACTIONS ON WIRELESS COMMUNICATIONS, IEEE TRANSACTIONS ON MOBILE COMPUTING, and IEEE TRANSACTIONS ON VEHICULAR TECHNOLOGY.

...